Enhanced geolocation of spaceborne laser altimeter surface returns: parameter calibration from the simultaneous reduction of altimeter range and navigation tracking data

S.B. Luthcke[a],*, C.C. Carabajal[b], D.D. Rowlands[a]

[a]NASA Goddard Space Flight Center, Laboratory for Terrestrial Physics, Space Geodesy Branch, Code 926, Greenbelt, MD 20771, USA
[b]NVI, Inc. @ NASA GSFC, Code 926, Greenbelt, MD 20771, USA

Abstract

The accurate geolocation of a laser altimeter's surface return, the spot from which the laser energy reflects on the Earth's surface, is a critical issue in the scientific application of these data. Pointing, ranging, timing and orbit errors must be compensated to accurately geolocate these data. Detailed laser altimeter measurement models have been developed and implemented within precision orbit determination software providing the capability to simultaneously estimate the orbit and geolocation parameters from a combined reduction of altimeter range and spacecraft tracking data. In preparation for NASA's future dedicated Earth observing spaceborne laser altimeter missions, the Vegetation Canopy Lidar (VCL) and the Ice, Cloud and land Elevation Satellite (ICESat), data from two Shuttle Laser Altimeter (SLA) missions have been reprocessed to test and refine these algorithms and to develop the analysis methodologies for the production and verification of enhanced geolocation products. Both direct altimetry and dynamic cross-over data have been reduced in combination with navigation tracking data to obtain significant improvement in SLA geolocation accuracy. Residual and overlap precision tests indicate a factor of two improvement over the previously released SLA Standard Data Products, showing 40-m RMS horizontal and 26-cm RMS elevation geolocation precision for the long SLA-01 arcs. Accuracy estimates by comparing SLA profiles to Digital Elevation Models show horizontal positioning accuracy at the 60-m (1σ) level. Vertical accuracies, on the order of 1 m (1σ) for low slope surfaces are now dominated by the ± 75-cm one-way range resolution of the instrument. Comparable relative improvements are also observed in the analysis of the SLA-02 data. The analyses show that complex temporal variations in parameters (i.e., pointing) can be recovered and not just simple biases. The methodology and results obtained from the detailed analysis are discussed in this paper, along with their applicability to VCL and ICESat. Published by Elsevier Science Ltd.

* Corresponding author. Tel.: +1-301-614-6112; fax: +1-301-614-6099.
  E-mail address: sluthcke@xyz.gsfc.nasa.gov (S.B. Luthcke).

1. Introduction

With the increasing number of airborne and space-based laser altimeter instruments, laser remote sensing is revolutionizing the ability to determine the characteristics of complex surfaces including vegetation height, slope, surface roughness and topography along with surface change detection. To take advantage of the unique observing capabilities of the lidar technology, two NASA dedicated Earth observing laser altimeter missions are scheduled for launch in the near future: the Vegetation Canopy Lidar (VCL) and the Ice, Cloud and land Elevation Satellite (ICESat). The ICESat mission will carry the Geoscience Laser Altimeter System (GLAS), which consists of three two-channel lasers to be operated sequentially over 3–5 years. The near-infrared channel will make precise elevation measurements of the ice sheets, sea ice roughness and thickness, ocean and land surface elevations and surface reflectivity. The surface spot size is 70 m in diameter spaced at 172 m along-track. These measurements will enable determination of present-day mass balance of the ice sheets, the study of associations between observed ice changes and polar climate, and the estimation of the present and future contributions of the ice sheets to global sea level rise (Zwally et al., 2002).

The VCL mission will carry a unique Multi-Beam Laser Altimeter (MBLA). The VCL MBLA is a three-beam instrument where each laser is capable of producing 25 m diameter surface footprints with 30 m along-track spacing from a 400 km altitude. VCL will provide the first and only global data set of the vertical structure of the Earth's forests, characterizing landcover for terrestrial ecosystem and climate monitoring, modeling, and prediction (Dubayah et al., 1997). The instrument is designed to operate for an expected mission duration of 2 years, measuring vegetation canopy heights and ground surface elevations with a vertical accuracy of less than 1 m (1σ, shot-to-shot), as well as recording the vertical distribution of intercepted surfaces (waveforms) (Dubayah et al., 1997). The VCL mission will address the most pertinent problems in the carbon cycle, quantifying the magnitude of deforestation and furthering our understanding of the current and future terrestrial carbon sink.

The ground spot size of these spaceborne laser altimeters is as small as the VCL footprint of 25 m, and is on the order of 20–80 times smaller than the footprint of spaceborne radar altimeters now in use (TOPEX, GFO, ERS-2). The returned waveform provides detailed information about the surface characteristics within each footprint. The small laser footprints and the small spatial scale over which the surface characteristics of interest vary, require precise geolocation, typically on the order of the size of a footprint or less. Since identifying the spot that is illuminated is critical when utilizing laser altimetry, laser bounce point geolocation is an important issue. One approach to spaceborne laser altimeter data geolocation is to independently obtain laser pointing, spacecraft body attitude, spacecraft orbit, range bias and time tag corrections and to simply combine these elements along with the range observation to obtain the geolocated surface return. However, these data have errors and their pre-launch parameter values and models must either be verified or more likely corrections must be estimated once the instrument is on orbit. Towards this end, the laser range observations can be fully exploited in an integrated residual analysis to accurately calibrate these corrections or geolocation/instrument parameters (Luthcke et al., 2000; Rowlands et al., 2000). Our "integrated residual analysis" is a technique that simultaneously estimates orbit and geolocation parameters from a combined reduction of laser range and spacecraft tracking data.

While this technique is not new for spaceborne radar altimetry, what is new is the implementation and application of the laser altimeter measurement models that take into account the additional complexities of the spaceborne laser altimeter observation. This integrated residual analysis is the primary calibration method for the VCL mission geolocation. Because the VCL on-orbit pointing, ranging, timing and orbit corrections will be solely determined from these techniques, the VCL science requirements and instrument characteristics have pushed the development of the range residual analysis techniques to their current level. ICESat has a dedicated instrument calibration and validation experiment along with a complex Stellar Referencing System (SRS) to precisely measure the orientation of each shot's pointing. However, the integrated residual analysis techniques will be applied to ICESat for an independent calibration and validation. In this paper we summarize the laser altimeter measurement model algorithms and their implementation, and the integrated range residual analysis techniques. These capabilities are then fully tested using a detailed analysis of the data from two Shuttle Laser Altimeter (SLA) missions. The methodologies developed and the geolocation improvements obtained are presented along with a brief discussion on the applicability to VCL and ICESat.

2. Geolocation and instrument parameter calibration methodology and algorithms

Because of the small ground footprint of the laser altimeter, small pointing errors will induce large horizontal geolocation errors, as compared to the footprint size, even for small deviations from nadir (Luthcke et al., 2000). Pointing errors are typically the dominant error source for horizontal positioning, and are significant contributors to height errors in moderately to highly sloping terrain (Bufton, 1989; Gardner, 1992). A representation of the laser range geometry can be found in Fig. 1. The sensitivity of the computed laser range to pointing errors can be expressed as:

$$\sigma_\rho = \frac{h\tan(\theta + S)}{\cos(\theta + S)}\sigma_\theta \tag{1}$$

σ_ρ = standard deviation of one half of the laser altimeter two-way range observation, m
h = height above surface, m
θ = off-nadir angle
S = surface slope
$\theta + S$ = surface incidence angle
σ_θ = standard deviation of the off-nadir angle

The significance of pointing error can be easily understood using the expression in Eq. (1) and the example in Luthcke et al. (2000). The VCL laser-detector coboresight alignment budget allows for possible misalignments on the order of 30 arc-s. We now consider this 30-arc-s misalignment bias for a 400-km altitude instrument with a very moderate 1° laser-pointing surface incidence angle (includes both surface slope and off-nadir pointing). In this case, the resultant geolocation error will be 58 m horizontally and 1 m in height. For ICESat, a 600-km altitude instrument, the errors are 87 m horizontally and 1.5 m in height. These errors far exceed the mission requirements for only one error source with a very moderate surface incidence angle.
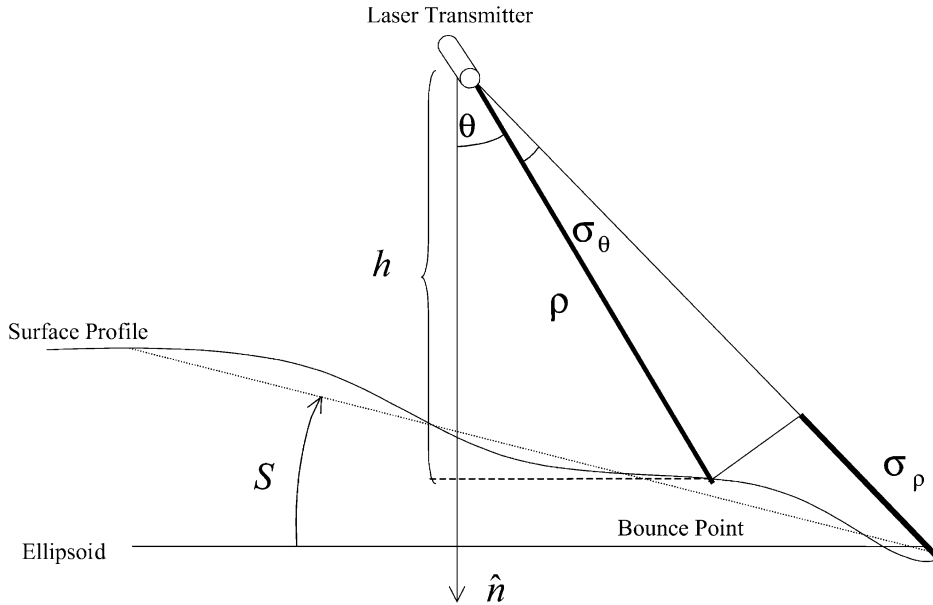
Fig. 1. Laser range geometry (Luthcke et al., 2000).

While large footprint, ocean surface observing, radar altimeter range data can be processed with the simplifying assumptions of geodetic pointing, laser altimeter measurement models must precisely consider the pointing of the instrument, the small footprint and the highly varying surface characteristics from which the data is collected.

The laser altimeter range measurement model algorithms have been implemented within NASA/Goddard Space Flight Center's (GSFC) GEODYN precise orbit and geodetic parameter estimation system (Pavlis et al., 1999). Therefore, the laser altimeter range processing can take advantage of GEODYN's reference frame modeling based on International Earth Rotation Service conventions, detailed geophysical modeling and its formal estimation process. The estimated parameters are solved for iteratively using a differential correction Bayesian least-squares estimation. The differential correction to the estimated parameter value (true solution approximation) on the nth iteration is given by the Bayesian parameter estimation formula:

$$\mathrm{d}\mathbf{x}^{(n+1)} = \left(B^T W B + V_A^{-1}\right)^{-1}\left[B^T W \mathrm{d}\mathbf{m} + V_A^{-1}\left(\mathbf{x}_A - \hat{\mathbf{x}}^{(n)}\right)\right]$$

where: $\mathrm{d}\mathbf{x}$ is a vector of the differential corrections to the estimated parameters, B is the matrix of partial derivatives of the observations with respect to the parameters, W is the weighting matrix associated with the observations, V_A is the *a priori* parameter covariance matrix, $\mathrm{d}\mathbf{m}$ is the vector of residuals (observed −computed) from the nth approximation, X_A is the *a priori* estimate of the true state solution vector, $\hat{\mathbf{x}}$ is the approximation to the true state solution vector. The estimate of the state after the $n+1$ iteration is given by:

$$\hat{\mathbf{x}} = \hat{\mathbf{x}}^{(n)} + \mathrm{d}\mathbf{x}^{(n+1)}$$

The error in the estimated parameters is then given by:

$$\Delta \mathbf{x} = \hat{\mathbf{x}} - \mathbf{x}$$

The GEODYN implementation allows for the simultaneous estimation of the geometric and dynamic parameters of the orbit and laser range measurement model through the reduction of a combination of spacecraft tracking and laser altimeter range data residuals.

Three laser altimeter measurement models have been implemented within the GEODYN system. The first is a rigorous implementation of the classic geolocation measurement model that takes into account the motion of the laser tracking points over the round trip light time of the laser pulse. The model computes both transmit and receive leg ranges to precisely geolocate the surface return. Although the geolocation model cannot be used directly to estimate parameters, it is used in constructing the "dynamic crossover" measurement model discussed below, and provides a standardized geolocation file for any particular solution. The geolocation file includes the location of the surface return in geodetic and Earth Centered Fixed (ECF) cartesian coordinates along with a host of media and geophysical corrections. The geolocation file also contains information about the laser orientation, range and time tag biases.

The second measurement model implemented is an altimeter "crossover" capability, which we term "dynamic crossovers" (DXO). This crossover measurement model has been implemented to take into account the small footprint of the laser altimeter along with the observed sloping terrain, and therefore, the horizontal sensitivity of these data. The DXO measurement model is discussed in detail along with its application to orbit and attitude determination for Mars Global Surveyor (MGS) in Rowlands et al. (1999). The altimeter observations from both the ascending and descending passes surrounding a crossover point trace out two curves in space. These curves contain the signal from topography, orbit, laser pointing, range and timing parameters. Three-dimensional polynomials are used to represent the ascending and descending curves. The crossover pair of observations, and their times, are found at the minimum distance between the curves. The crossover distance is minimized through the estimation of orbit, laser pointing, range and timing parameters. The formulation can exploit change in horizontal crossover location as well as change in radial position of the satellite. As the solution changes from iteration to iteration, it is likely that the crossover pair of observations will change and hence the name "dynamic crossovers". This capability has been used to significantly improve MGS orbit and attitude solutions as discussed in Rowlands et al. (1999).

The third measurement model implemented is the "direct altimetry" (DA) measurement model. The round trip range is computed using knowledge of the spacecraft position, laser pointing, timing and ranging parameters along with surface height. GEODYN has the capability to ingest multiple surface height grids representing various land areas and the ocean surface. The observed ranges are compared to those computed from the measurement model. The discrepancies between the observed and computed observations (i.e., the residuals) are minimized through the estimation of orbit, pointing, timing and ranging parameters. A detailed discussion and mathematical description of the direct altimetry measurement model is presented in Luthcke et al. (2000).

The current GEODYN implementation supports Multi-Beam-Laser-Altimeters (MBLA), like that to be flown on VCL, as well as single beam instruments like ICESat's GLAS. The following geolocation parameters can be estimated: laser range observation time tag bias, spacecraft

attitude time tag bias, range observation bias and scale and laser pointing parameters. These parameters can be recovered on a time period basis where different parameter sets can be estimated for each distinct time period within a data-reduction arc. Multiple time periods of user-defined length can be employed. The pointing parameterization is detailed in Luthcke et al. (2000). However, for completeness, it is sufficiently important to warrant the inclusion of this detail here.

The pointing of the laser in the Inertial Reference Frame (IRF) is modeled with a succession of rotations, each denoted by a rotational matrix R:

$$\hat{P}_{IRF} = R_{SBF \to IRF} R_{SBFC \to SBF} R_{Laser \to SBFC} \begin{bmatrix} 0 \\ 0 \\ -1 \end{bmatrix} \tag{2}$$

$\hat{P}_{IRF}$ = laser unit pointing vector in Inertial Reference Frame
$R_{SBF \to IRF}$ = Rotation, Spacecraft Body Fixed frame to Inertial Reference Frame
$R_{SBFC \to SBF}$ = Rotation, Spacecraft Body Fixed Corrected frame to SBF
$R_{Laser \to SBFC}$ = Rotation, Laser frame to SBFC

The time series of quaternions that represents the Spacecraft Body-Fixed Frame -to- IRF (SBF-to-IRF) rotations are provided by the post-processed spacecraft attitude sensor data (e.g., star-tracker and gyroscope). The first two rotation matrices, Laser-to-SBFC (SBF corrected) and SBFC-to-SBF, are specified by the user with a three axis Euler rotation in roll, pitch and yaw. The Euler angle representation was chosen since it is much more intuitive than a quaternion representation and, since the user has the flexibility to select the order of rotation, any singularities may be avoided. The current GEODYN parameterization for each of the Euler angles is shown in Eq. (3). This parameterization can be modified to represent the expected laser and startracker pointing variations and can be implemented as functions of telemetered temperature or pressure as well as time. The SBFC-to-SBF matrix provides the capability to estimate a misalignment correction to the spacecraft attitude knowledge (SBF-to-IRF). GEODYN has the capability to model a Laser-to-SBF rotation matrix for each of the N lasers, which comprise the complete instrument (e.g., VCL MBLA has 3 lasers). Only one SBFC-to-SBF matrix may be modeled.

$$\vartheta_{ij} = C_{ij} + D_{ij}\Delta t_j + Q_{ij}\Delta t_j^2 + A_{ij}\sin\omega\Delta t_j + B_{ij}\cos\omega\Delta t_j \tag{3}$$

ϑ = Euler angle (°)
C = Euler angle bias parameter (°)
D = Euler angle rate parameter (°/s)
Q = Euler angle quadratic parameter (°/s^2)
A = Amplitude of Euler angle sine term (°)
B = Amplitude of Euler angle cosine term (°)
ω = angular frequency, $(2\pi/T)$, where $T = 5545$ s for the SLA data analysis
Δt = elapsed time within current time period (s)
i = Euler angle index (1 = roll, 2 = pitch, 3 = yaw)
j = time period index

The implementation of the above laser altimeter measurement models within a single system that simultaneously supports the precision orbit determination process from multiple data types, facilitates a truly combined calibration approach for current and future spaceborne laser altimeter missions. Orbit and geolocation parameters can be simultaneously estimated from a combination of calibration data including direct altimetry from ocean surface and detailed calibration land site Digital Elevation Models (DEMs), and dynamic crossovers. While data from a few, small ($\sim$100 km pass length) detailed calibration sites provides an opportunity to estimate geolocation parameter biases for that particular time and location, by combining these data with global crossovers and long duration ocean sweeps we can further the accuracy and observe environmental and system related variations in the calibrated geolocation parameters (Luthcke et al., 2000; Rowlands et al., 2000). Both VCL and ICESat will use these capabilities for instrument parameter calibration and improved geolocation.

The integrated residual analysis is the primary method to be used for VCL geolocation parameter calibration, and is an independent method to be used to validate ICESat's Stellar Referencing System (SRS) laser pointing observations along with calibrating range and timing biases for both missions. Several pre-launch simulations and error analyses have been conducted to gauge the performance of these techniques. For example, Luthcke et al. (2000) details an extensive pre-launch error analysis and set of simulations to quantify the performance of "ocean sweep" maneuvers in recovering VCL and ICESat pointing and range corrections. The ocean sweep maneuvers exploit the relationship in Eq. (1), and use specific commanded spacecraft maneuvers and ocean DA range residuals for the recovery of the pointing and range parameters. Practical design considerations, the impact of various error sources and performance results are discussed. The paper shows (see *Consider-Covariance Analysis Results* section) how the recovery of pointing corrections can be made to the sub-arc-s level for a single maneuver under the worst expected conditions taking into account a detailed error model. The paper also shows (see *Simulation Analysis Results* section) how orbital period and laser "warm-up" temporal variations in the pointing misalignment can be recovered using the calibration maneuver and the resultant DA ranges.

While it is important to perform the various pre-launch error analyses and simulations, these pre-launch studies do not fully test the laser altimeter measurement model algorithms and processing software. Systematic errors in the software and algorithms can cancel and may not be detected in pre-launch simulations. In preparation for VCL and ICESat, it is imperative that these algorithms are rigorously tested. Complete testing includes the processing of actual Earth observing spaceborne laser altimetry to fully test the algorithms, reference frames and geophysical models. We make the distinction of testing spaceborne rather than airborne laser altimetry. The spaceborne laser altimeter measurement model algorithms must take into account the much greater vehicle velocity and light times (laser pulse travel time), precise reference frames and geophysical modeling, as well as the inclusion of the precision orbit determination process. The DXO algorithms have been successfully applied to orbit and attitude determination of Mars Global Surveyor (Rowlands et al., 1999). Still further testing is needed to verify the algorithms for the processing of an Earth orbiting laser altimeter's data in conjunction with the DA algorithms and to verify the application of inter-mission crossovers. Furthermore, in addition to the DXO algorithm, the DA measurement model algorithm needs to be fully tested and verified. Towards this end, the data from two Shuttle Laser Altimeter missions (SLA-01 and -02) have been

reprocessed applying these new measurement model algorithms to obtain an Enhanced Data Product (EDP) geolocation which represents a significant improvement over the current SLA Standard Data Products (SDP) (Garvin et al., 1998; Carabajal et al., 1999). The details of this analysis and the results obtained are discussed in the following sections of this paper.

3. SLA geolocation parameter estimation and resultant enhanced geolocation

In order to rigorously test the GEODYN implementation of the laser altimeter measurement model algorithms and capabilities we have reprocessed a total of 37 h of SLA-01 observations and nearly 13.5 h of SLA-02 data. This represents approximately 50% of the SLA-01 and 23% of the SLA-02 data originally processed (Garvin et al., 1998; Carabajal et al., 1999). The observation periods selected represent those that do not contain any significant attitude and orbit maneuvers and, for the case of SLA-02, do not exhibit any significant waveform problems. Future laser altimetry data from geodetic satellites such as VCL and ICESat will not have these Shuttle/ SLA specific issues to address, therefore, any generalizations derived from the analysis of these arc selections are still valid for the algorithm and methodology testing. In total, three 9-h and one 10-h SLA-01 observation periods, and three 3-h and one 4.5-h SLA-02 observation periods were reprocessed. During these periods the Shuttle was in a -ZLV (-Z axis along Local Vertical),-XVV (-X axis along the Velocity Vector) or -YVV Local Vertical Local Horizontal (LVLH) attitude mode. The Shuttle remained in a 1° attitude "dead-band" where the orientation for each fundamental spacecraft axis (roll, pitch, yaw) remained within 1° of the nominal attitude [see Rowlands et al. (1997) for more detail].

SLA is a hybrid instrument that combines the MOLA (Mars Orbiter Laser Altimeter) electronics with a high-speed digitizer capable of recording the amplitude versus the time history of backscattered laser energy (the waveform). The waveform is a measure of the height distribution of illuminated surfaces within the 100-m diameter SLA footprint. The SLA operates at 0.1 Hz producing an observation every 0.7 km along-track from a 300-km orbit. The altimeter measures the distance between the instrument and the backscattering surface by timing the two-way travel of the 10 ns, 1064-nm optical wavelength, laser pulses. A leading-edge, threshold-crossing, round-trip range observation is made from the detection of the leading edge of both the transmitted pulse and the backscattered received pulse when the signal is above a certain threshold. The timing resolution of the transmitted (start) and receive (stop) pulse is limited by the least significant bit of the instrument's high-resolution digital counter. The SLA Time Interval Unit (TIU) basic resolution is 10 ns, which corresponds to ±0.75 m in one-way range resolution (Garvin et al., 1998). The TIU leading-edge threshold crossing corresponds to the highest "perceived" surface within the laser footprint, assuming the return is of sufficient area and reflectivity to return a signal above detection level. When a return pulse is detected the 250 MHz digitizer records an electronic representation of the shape of the backscattered return. The shape of the received pulse is translated to digital samples with a resolution of 2–10 ns (see http://dena-li.gsfc.nasa.gov:8001/). The TIU ranging result needs to be tied to the digitized waveform signal. For SLA, the correspondence between the waveform bin position and the TIU stop event is not constant, but examination of the waveforms revealed the position in which the received signal

first exceeded the background noise level of the waveform (Carabajal et al., 1999). Although not necessarily identical to the TIU stop pulse event, it should be considered essentially equivalent.

Time-tagging the 10 pulses-per-second (pps) SLA observations involved synchronizing the SLA internal clock with the orbiter's clock. The Shuttle's clock gives an absolute reference to the Mission Elapsed Time (MET), while the SLA clock provides an incremental measure of time for the instrument. The Shuttle's MET is not allowed to deviate by more than ± 10 ms from the absolute time kept at the ground station. However, this time is often much better than 10 ms because frequent updates are made where the accuracy of these updates is kept within ± 5 ms (Hitchhiker CARS, 1994). The SLA software receives a 1-min time tag from the Shuttle Master Time Unit (MTU) for the purposes of synchronizing SLA's internal clock to an absolute time reference. An inexpensive oscillator (standard for the flight computer, with a 1.193-MHz frequency) is used to keep SLA internal time. The offset between the Shuttle 1-min timing signals and the SLA internal clock are used to remove SLA clock oscillator drift errors along with a simple timing bias.

3.1. Reduction of direct altimetry and tracking data

The dominant systematic error sources contributing to the SLA data geolocation are laser pointing, radial orbit, range bias or system delay and observation time tag errors. Uncorrected, the pointing errors constitute kilometer-level horizontal errors and tens of meters vertical error during the 1° attitude dead-band. A preliminary method of extracting only roll and pitch constant biases has been used to compute the SLA Standard Data Product (SDP) geolocation. This method compares sea surface height from a Mean Sea Surface (MSS) to the SLA ocean geolocated ellipsoid heights, and a simplified formula is used to derive the resulting pointing (Garvin et al., 1998). This method is not capable of extracting higher order pointing errors and cannot contribute to the simultaneous estimation of the orbit and range bias parameters. In Luthcke et al. (2002) a preliminary analysis of the application of the GEODYN direct altimetry algorithms to the simultaneous estimation of orbit and pointing geolocation parameters indicates significant improvement in geolocation accuracy can be achieved. However, that study had only considered a very limited solution for a single SLA-01 observation period. In this paper we present a complete enhanced geolocation detailed analysis using an appropriate sampling of the SLA data.

The 90 m accuracies (1σ) of the nominal post-flight shuttle orbit made it necessary to perform an alternative precision orbit determination (POD). The Shuttle POD method used has been well documented in Rowlands et al. (1997). Both Tracking and Data Relay Satellite System (TDRSS) and Global Positioning System (GPS) tracking data were available for STS-72 (SLA-01) and STS-85 (SLA-02) POD. The only continuous GPS observations available for these missions were 4–5 channels of L1 pseudorange data from both a Collins 3M (for STS-72) and a Boeing MAGR (for STS-85) receiver. Shuttle POD computed from this GPS data alone, or from a combination of this GPS data and the available TDRSS tracking data, showed no significant radial orbit precision improvement over TDRSS-based Shuttle POD (Rowlands et al., 1997). The radial direction is the dominant orbit error component affecting geolocation accuracy. The first-order effect is a direct mapping of the radial orbit error to vertical positioning. The second order effect comes from radial orbit error contributing to the pointing parameter calibration error and therefore affecting the horizontal positioning error as can be seen from Eq. (1). The few meters of

shuttle horizontal orbit error are a small percentage of the 100-m footprint and tens of meters of horizontal pointing error. Therefore, only TDRSS two-way range-rate tracking data are used (along with the laser altimeter ranges) in the Shuttle POD considered in this paper.

Highly precise TDRS orbits are determined through rigorous force and measurement modeling and the inclusion of TDRSS tracking of TOPEX/Poseidon (T/P) (Luthcke et al., 1997). The centimeter level of T/P's orbit accuracy makes it a precisely located roving tracking station that, when added to the TDRS orbit determination, greatly improves the resultant TDRS orbit accuracies. Using this method, meter-level total position TDRS orbit accuracies can be achieved, which is a significant improvement over the 30–60 m operational orbit accuracies (Luthcke et al., 1997). Still further improvements in TDRS orbit performance were achieved in support of STS-85. In preparation for this mission an optimal TDRS-T/P (TDRS -to- T/P) tracking scenario was developed and applied. The result was an evenly distributed, dense TDRS-T/P tracking data set which, when reduced in conjunction with our detailed TDRS force and measurement models, resulted in sub-meter (87 cm RMS) total position orbit precisions as obtained from orbit overlap comparisons. The impact of this greatly improved TDRS orbit performance is that the contribution of TDRS orbit error to Shuttle orbit error has been significantly reduced to less than 5 cm (radial RMS) for the Shuttle.

The Shuttle POD employs a batch processing reduced dynamic solution technique, which is described in detail in Rowlands et al. (1997). The orbit parameters estimated include: the six initial state parameters, a single drag coefficient (C_D) per arc, and the amplitude and phase of an along and cross track one-cycle-per-rev (OCPR) empirical acceleration every quarter of an orbit period. The details of the nominal force and measurement modeling can be found in Rowlands et al. (1997). As a first step in improving the SLA geolocation accuracy, nominal Shuttle orbits (those computed from the tracking data only) were recomputed with several enhancements: EGM96 geopotential, TDRS macro-model, improved TDRS tracking data editing, improved covariance constraint parameterization. The optimal parameterization, including the covariance constraint weighting parameters (correlation time and standard deviation) were determined using tracking data residuals and orbit overlap discrepancies as the performance indicators. While the details and results of these tests will be discussed in the following sections, we do note here that the resulting radial precision of the reprocessed nominal Shuttle arcs shows nearly a factor of 2 improvement over the SLA SDP orbit performance found in Rowlands et al. (1997).

The direct altimetry measurement model is evaluated using the orbits discussed above, instrument tracking point offsets corrected for attitude and center of gravity (cg) variations, range and surface modeling corrections, and laser pointing constructed as in Eq. (2). The Shuttle SBF-to-IRF rotation is constructed from telemetered quaternions obtained using Johnson Space Center's Mission Evaluation Workstation (MEWs) software. In this study, only deep ocean (depths greater than 1 km) direct altimetry observations were used in the recovery of geolocation parameters to eliminate large modeling errors near the coasts. The sea surface height (SSH) is modeled using the Ohio State University Mean Sea Surface 95 (OSU MSS 95) (Yi, 1995). The temporal variations due to Earth tides, pole tide, ocean tides and ocean loading were included. The Goddard Ocean Tide 99 model (GOT99) was used (Ray, 1999). The ranges are corrected for tropospheric effects and the *a priori* system delay measured in the laboratory (5.6 m) (Bufton, pers. comm.). The surface height variations due to barotropic pressure variations and time dependent dynamic topography were ignored. For SLA-01 and SLA-02, which were at a 28.5 and

$57°$ orbit inclination, the surface height omission errors due to changes in barotropic pressure are less than 5 cm for SLA-01 and less than 12 cm for SLA-02 (Fu and Pihos, 1994). The omission errors from neglecting temporal variations in deep ocean dynamic topography is on the order of 11 cm (1σ) (Yi, 1995; Wunsch and Stammer, 1995). Therefore, in light of the ±75-cm one-way ranging resolution of the TIU range and the dominant orbit and pointing errors, it is reasonable to neglect these errors for the purposes of this algorithm validation analysis. The direct altimetry processed (unless otherwise stated) was decimated by a factor of 10 to ease computational burden for this algorithm testing, and to match the minimum number of observations to be processed from an ocean sweep calibration maneuver (Luthcke et al., 2000). Limited tests to compare solutions using full-rate versus the decimated ocean direct altimetry showed differences only within the expected precisions of the solutions.

Leading-edge detected ranges were used in the geolocation parameter estimation. These observations may suffer from range walk errors, which are the result of differences in surface characteristics (i.e., albedo, incidence angle and roughness) varying the return pulse amplitude and shape, which in turn will change the location of the leading-edge threshold crossing. However, deep ocean returns are used in the parameter recovery where the surface characteristics remain somewhat constant thereby minimizing the range walk error. To test the affects of range walk errors on the ocean surface range observations and to compute the range to the mean ocean surface and the lowest elevation represented in the waveforms for land, the SLA-02 data has been reprocessed with ranges that have been corrected using the information contained in the returned waveform.

3.1.1. SLA-01 results

The longest continuous SLA observation periods, with good TDRSS tracking data distribution, were initially processed to find the optimal data weighting and arc parameterization. These arcs include three 9-h SLA-01 observation periods (1, 3s and 4). Both data residuals and overlap (orbit and geolocation) comparisons are used to discriminate between the various solution scenarios. To compute overlap comparisons each SLA-01 observation period is split into two arcs that overlap by two orbit revolutions (3 h) for these long 9–10 h arcs. Each overlapping arc is then independently reduced and both orbit solutions and geolocated bounce point positions are differenced during the overlapping time period. Using the precise geolocation measurement model and the converged orbit, pointing and range bias solution, the position of the surface return bounce point is computed in latitude, longitude and ellipsoid height. Similar to orbit overlap tests, each arc's overlapping geolocated surface return positions are then differenced. The orbit overlap comparisons provide an indication of the precision of the orbit solution, and the geolocation overlap comparisons provide a gauge of the orbit, pointing, timing and range bias parameter solution precision. How well these overlap tests represent solution precision is dependent on how short the overlapping period is in comparison to the individual arc lengths and on whether there is enough variability over the solution span to make the two solutions independent. The choice of overlapping time period duration was a compromise between having a good multiple orbit revolution sampling for the overlapping time period, and minimizing the ratio of the overlap duration to the arc length. While our somewhat large overlap duration may compromise this test as an exact indicator of solution precision, it does not minimize its usefulness as a performance discriminator between solutions.

Fig. 2 shows the very large 11 m RMS and 30 m maximum range residuals that are obtained if the pointing and range bias are not estimated (anpnt solution). Also, from Fig. 2, we can see that the ocean surface residuals are a good indicator of geolocation accuracy because they represent the vertical error of the measurement. Coupled with the varying attitude about nadir (shuttle roll and pitch shown in Fig. 2), they provide insight into the extent of probable pointing errors and therefore horizontal errors. Fig. 2 illustrates how the relationship shown in Eq. (1) can be exploited to estimate pointing corrections as well as orbit and range bias parameters from the reduction of ocean direct altimetry (DA) residuals. While not an optimal calibration maneuver like those to be performed for VCL and ICESat, the Shuttle 1° attitude dead-band does provide enough amplitude and orientation separation to simultaneously estimate roll and pitch laser pointing corrections along with range bias and orbit parameters (Luthcke et al., 2000).

Several combinations of data weighting and solution strategies were investigated. Results from the more important of these solution scenarios are presented in Table 1 (overlap comparisons) and Table 2 (residuals). Results from using the pre-launch *a priori* pointing and ranging bias are not included in Table 2 because they exhibit very poor performance (see anpnt solution in Fig. 2). Solutions 1a and 2a are obtained from Shuttle orbits determined from TDRSS tracking only and then held fixed while the pointing and range bias parameters are estimated using the ocean DA range data. Solutions 3a–5a represent those solutions where a combined reduction of TDRSS tracking and laser altimeter range data are used for the simultaneous estimation of orbit, pointing and range bias parameters. Solution 1a is a significant improvement over geolocation computed
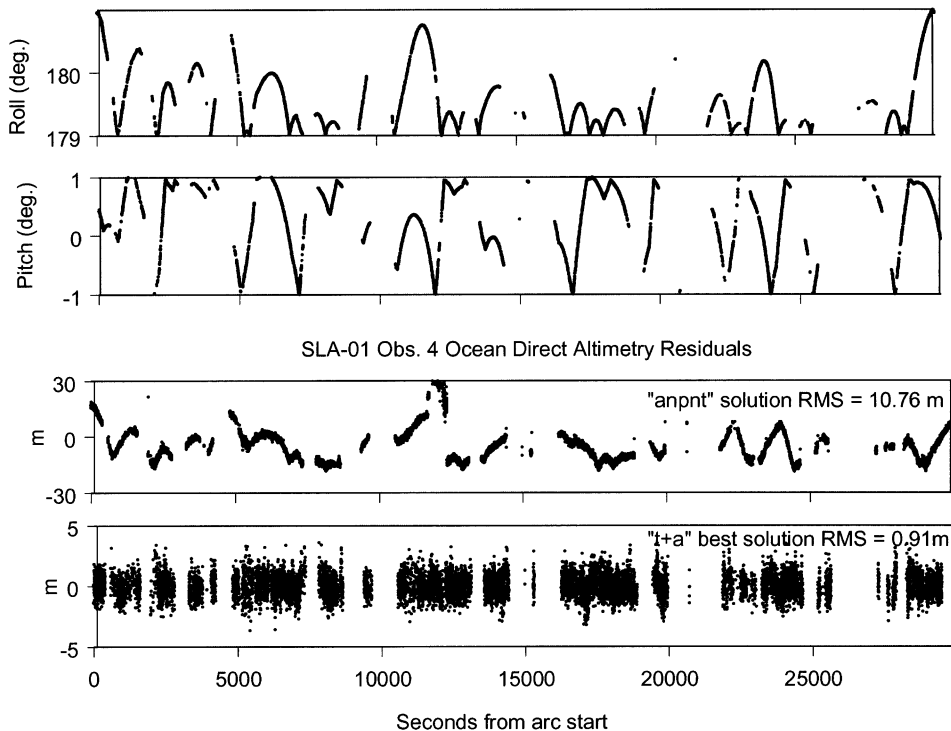

Fig. 2. SLA-01 observation period 4 attitude dead-band and ocean direct altimetry residuals.

using the *a priori* pointing and range bias. In this solution only constant and linear rate roll and pitch laser pointing corrections (termed "simpatt") are estimated [see Eq. (3)]. The constant term accounts for systematic misalignment of the laser while the linear rate accounts for the drift of the Shuttle Inertial Measurement Unit (IMU) over the observation period. This solution is the most similar to the SLA geolocation SDP. However solution 1a does represent an improvement over the SDP due to the enhanced nominal Shuttle orbits, and the simultaneous estimation of both range bias and a pointing linear rate, as well as estimating the constant pointing corrections.

In addition to the constant and linear rate pointing errors, quadratic and pointing errors that vary at orbital period were suspected. The quadratic term accounts for additional complexity in the IMU drift, while the periodic pointing errors are due to spacecraft body flexure and variations in the pointing due to instrument thermal gradient variation. Instrument telemetered temperature data indeed showed strong orbit period variation in temperature gradients. For solution 2a, range bias along with roll and pitch constant, rate, quadratic and orbit period correction parameters

Table 1
SLA-01 (data from observation periods 1, 3 and 4) orbit and geolocation overlap performance for various solution techniques

Solution			Orbit Overlap (RMS)		Geolocation Overlap (RMS)		
Solution number	Data	Parameters Estimated	Radial (m)	Total (m)	Ht. ocean (m)	Ht. land + ocean (m)	Horiz. (m)
1a	a	simpatt + rbias	0.54	3.73	0.76	1.02	93.24
2a	a	fullatt + rbias	0.54	3.73	0.78		87.25
3a	t + a	simpatt + rbias + orb.	0.78	3.10	0.38	0.73	49.92
4a	t + a	fullatt + rbias + orb.	0.32	2.86	0.12	0.26	39.54
5a	t + a + xtp	fullatt + rbias + orb	0.31	2.87		0.26	39.21

a,   ocean direct altimetry;
t + a,   TDRSS 2wrr and direct altimetry;
t + a + xtp,   TDRSS 2wrr, direct altimetry and SLA-TOPEX crossovers;
simpatt,   roll and pitch constant and rate;
rbias,   range bias;
fullatt,   roll and pitch constant, rate, quad. and one cycle per rev (OCPR);
orb.,   orbit pos. + vel., Cd per arc, along and cross OCPR empirical accelerations per quarter rev.

Table 2
SLA01 (data from observation periods 1, 3 and 4) tracking data, ocean direct altimetry and inter-and intra- mission dynamic crossover residual performance for various solution techniques

Solution			Data Fit RMS			
Solution number	Data	Parameters Estimated	TDRSS 2wrr (cm/s)	Direct Alt. (m)	X-over TOPEX (m)	X-over SLA (m)
1a	a	simpatt + rbias	0.214	1.93	1.75	
2a	a	fullatt + rbias	0.214	1.32		
3a	t + a	simpatt + rbias + orb.	0.247	0.98		
4a	t + a	fullatt + rbias + orb.	0.223	0.89	0.62	0.99
5a	t + a + xtp	fullatt + rbias + orb	0.221	0.89	0.60	

were estimated; pointing parameters C, D, Q, A and B in Eq. (3) for both roll and pitch (termed "fullatt"). While the solution 2a DA residuals show significant improvement (Table 2) over the solution 1a residuals, the geolocation overlap results (Table 1) show only marginal improvement. Furthermore, the residuals still showed evidence of orbit and pointing systematic errors.

In order to reduce these errors, we next performed a series of solutions in which orbit, pointing and range bias parameters were estimated from a combined reduction of DA and TDRSS tracking data. The optimal orbit parameterization determined in the tracking data only solutions was used in these combination solutions. The optimal pointing parameterization and data weighting (0.2 cm/s for TDRSS tracking and 0.75 m for laser altimeter range data) were then determined from a series of solutions using the resulting residual and overlap performance as a discriminator. Combination solution 3a shows further significant improvement in the direct altimeter range residuals with some degradation in the TDRSS tracking data residuals. Solution 3a also shows significant improvement in geolocation overlap performance. Because the ocean range data are used in the parameter estimation, we see the ocean overlap height discrepancies are much smaller than those that include land (Table 1). However, since the application of these data is mostly for land-based science, we have included these data as a relevant statistic and also to understand the performance outside of the data used to constrain the solution. While the altimeter range residuals and geolocation overlap performance has greatly improved with solution 3a, there is a significant degradation in radial orbit overlap performance. In order to get both radial orbit overlap and geolocation overlap to improve with the solution 3a parameterization, the altimeter range data had to be significantly down-weighted (from a sigma of 0.75 to 20–30 m). Even then, the geolocation overlap performance suffered so much that the resulting orbit and geolocation performance was only a slight improvement or no difference over solution 2a.

Due to the low altitude and low amplitude, non-optimal (roll and pitch not 100% uncorrelated) pointing variation about nadir (1° attitude dead-band), the Shuttle orbit errors were likely aliasing themselves into the periodic pointing parameters thereby limiting the performance of solution 2a. In the combination solution 3a, the opposite scenario is likely happening whereby the periodic pointing errors are aliasing into the orbit parameters. The optimal solution (4a) is one that simultaneously estimates the orbit parameters and the "fullatt" pointing parameters [C, D, Q, A and B of Eq. (3)] along with range bias in a combined reduction of the laser range and tracking data. In the case of solution 4a, orbit, geolocation and residual performance have all been significantly improved. Furthermore, the TDRSS tracking residual performance has been improved over solution 3a, which is further indication that solution 4a represents an orbit improvement. Solution 4a represents a 41% improvement in radial orbit precision, a 74% improvement in geolocation height precision, and a 58% improvement in geolocation horizontal positioning precision over solution 1a. Over a factor of two improvement has been gained in ocean DA residual performance. A plot of the solution 4a recovered pointing correction for observation period 4 is provided in Fig. 3 and shows the very large constant, rate and periodic correction that must be accounted for to obtain accurate geolocation. This analysis shows that complex temporal variations in geolocation parameters, not just biases, can be recovered from these techniques. A simple propagation of the recovered pointing parameter formal standard deviations gives the maximum noise only total pointing uncertainty of ~30 arc-s, where pitch is slightly better determined than roll due to the earth-orbit induced range variation. At 300 km, this pointing error will produce ~40 m of horizontal uncertainty, agreeing with the horizontal geolocation overlap test results.

The range bias is estimated on an arc-by-arc basis. The average and standard deviation of the recovered range bias over all arcs studied (observation periods 1, 3s, 4 and 7) is 6.12 ± 0.28 m as compared to the 5.6 m measured in the laboratory. The average range bias formal uncertainty is 3 cm. The recovered range bias average and standard deviation for observation periods 1 and 3s is 5.88 ± 0.13 m, while that for observation periods 4 and 7 is 6.36 ± 0.02 m suggesting a distinct change in the range bias during the mission.

Fig. 2 shows the observation period 4 combined solution 4a (labeled "t+a" best) ocean DA residuals. The ocean residual frequency distribution, over all SLA-01 observation periods studied,
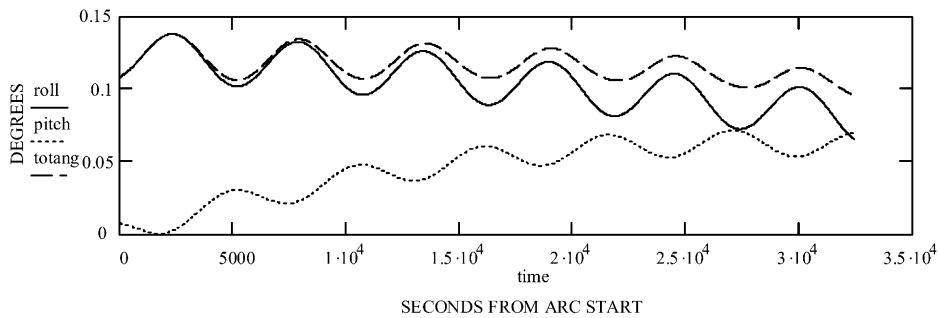

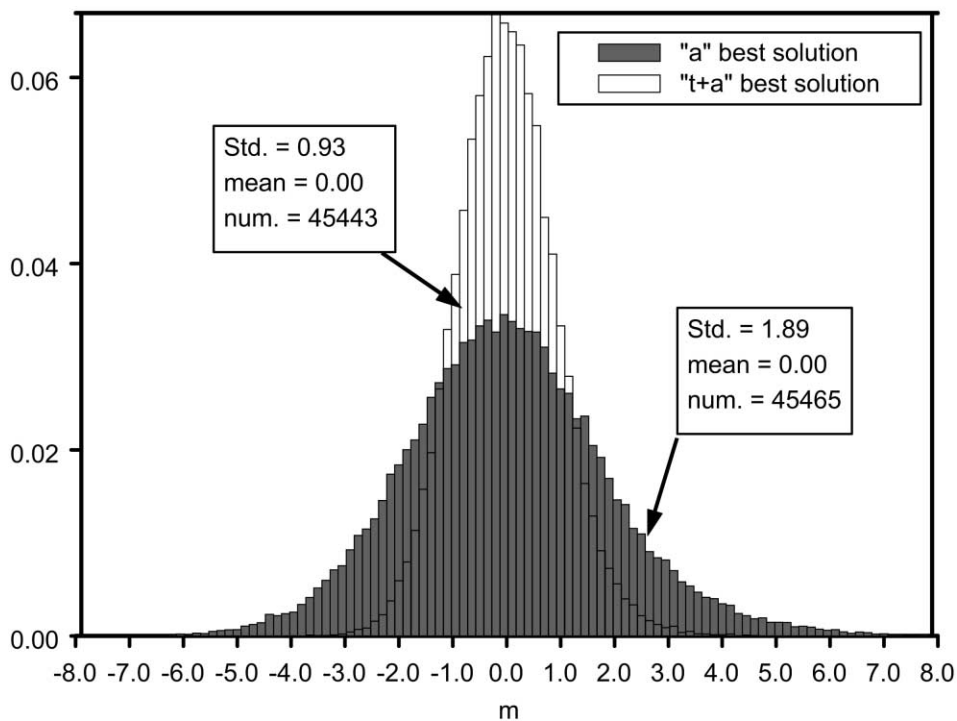Fig. 3. SLA-01 observation period 4 recovered pointing correction.

Fig. 4. SLA-01 ocean direct altimetry residual frequency (data from observation periods 1, 3s, 4 and 7).

is presented in Fig. 4. The significant improvement in residual performance obtained from the combined solution 4a technique is evident. In Behn and Zuber (2000), SLA-01 SDP (similar to solution 1a) geolocated ocean surface returns were compared to MSS and tides for several ocean profiles. For profiles from 1° attitude dead-band observation periods, the authors were able to achieve 1.03–1.24 m RMS agreement only after the removal of a mean, trend and frequencies $\leqslant$ 4/orbit-period in an attempt to account for the unmodeled systematic errors in the SLA SDP. The combined solution 4a residual performance of 0.93 m RMS is an improvement over these results and is applicable over all ocean data, not just selected profiles. Behn and Zuber's study points out that by empirically removing the long-wavelength variations in the residuals, much of the dynamic topography signal may inadvertently be removed from the data. However, the technique used here (solution 4a) minimizes this problem by accounting for the errors as they physically exist, recovering orbit, pointing and ranging parameters, while constraining the orbit adjustment by simultaneously reducing tracking data along with the altimeter range observations. Behn and Zuber (2000) attribute the source of the dominant 3/orbit-period signal in the residuals as possibly due to low degree orbit errors in the geopotential. However, from the present analysis, the periodic signal in the SLA-01 SDP surface return geolocation is due to a combination of orbit error and rate and periodic pointing error modulated by the temporal variation in spacecraft attitude. As can be seen from Fig. 4 and Table 1, these modeling errors have now been properly accounted for in the combined solution 4a.

For ocean data profiles from 0.1° attitude dead-band observation periods, Behn and Zuber (2000) show the residual agreement achieved, after empirical removal of the trends, ranges from 0.89 to 0.95 m RMS. These range residual results are essentially free of pointing error because the ranging errors due to pointing errors are minimized at small off-nadir pointing angles (during the 0.1° attitude dead-bands), as illustrated by Eq. (1). However, while the range residuals from these low off-nadir angle attitude profiles are essentially pointing error free, significant pointing error still exists in the horizontal geolocation. That is why the large attitude dead-band periods are actually more desirably because one can remove the pointing error from both the range and the horizontal positioning. These 'pointing error free' results agree with the 0.93 m residual RMS performance achieved in this study (Fig. 4), indicating that the pointing errors have been significantly reduced in the combined solution 4a geolocation for the 1° attitude dead-band observation periods.

Full-rate DA ocean residuals from all ocean returns (not just deep ocean) for observation period 3s were smoothed to remove the ranging noise. The resultant smoothed residuals have 24–34 cm RMS variability depending on the smoothing technique. This remaining error is mostly comprised of orbit error and SSH modeling error including the omission of temporal variations in the dynamic topography. The SSH modeling error is especially true since we have included all valid ocean data returns, in this particular comparison, and not just deep ocean data. Other error sources include: omission of the inverted barometer (IB) correction, ranging errors due to sea state and remaining pointing errors. The overlap performance presented in Table 1 indicate radial orbit precision is on the order of 12 cm RMS over oceans, 26 cm RMS over land and ocean, and 32 cm RMS over the entire arc (indicating tails in the overlap comparisons at the ends of the arcs). While an argument can be made that these results are optimistic and relate only to precision, the laser altimeter residuals provide a measure of radial orbit accuracy. Therefore, the overlap comparisons and the smoothed altimeter range residuals indicate that the radial orbit

accuracies are better than 30 cm RMS. This result compares favorably with Shuttle orbits computed using data from two JPL dual frequency BlackJack receivers in support of the Shuttle Radar Topography Mission (SRTM) onboard STS-99 (Bertiger et al., 2000). These STS-99 BlackJack-based orbits have average radial orbit overlap differences of 39 cm RMS, where the tails of the overlaps have been edited (Bertiger et al., 2000).

Fig. 5 summarizes the combined solution overlap performance for each of the observation periods studied. The results from the three observation periods with good TDRSS tracking, discussed above, along with observation period 7 are presented. Radial overlap and surface return height, for ocean data and for ocean and land data, RMS overlap discrepancies in cm are presented along with surface return horizontal positioning RMS overlap discrepancies in m. The observation period 7 degraded overlap performance is due to poor TDRSS tracking data distribution during this observation period. The poor tracking data distribution causes degraded orbit precision, which then affects the pointing parameter recovery. Only constant and rate pointing parameters were estimated in the observation 7 combined solution due to the poor tracking data distribution which degraded the ability to separate pointing and orbit parameters. Even so, the observation 7 combined solution results represent a geolocation precision improvement over the SLA-01 SDP geolocation or solution 1a: 60% improvement in ocean surface return height, 5% improvement in land and ocean surface return height and 30% improvement in horizontal positioning precision. Tails at the ends of the arc overlap period dominate the larger observation period 7 radial orbit overlap. A 42% improvement in direct altimeter range residual RMS is obtained from the combined observation period 7 solution.

3.1.2. SLA-02 results

SLA-02 gathered range and waveform observations from a~300-km altitude and a 58.5° inclination. Four observation periods representing 13.5 hours of SLA-02 data were also reprocessed in this study. Four 1° attitude dead-band observation periods were studied: obs. 1 (~3 h),
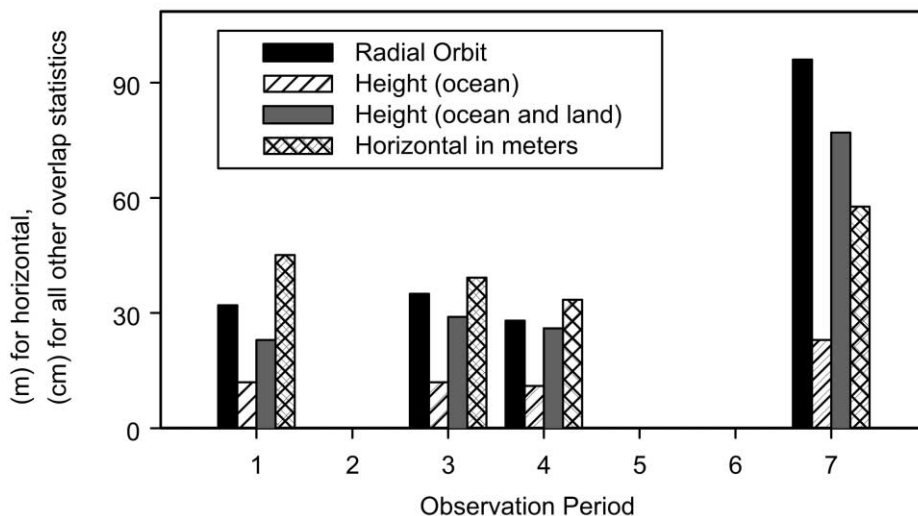

Fig. 5. SLA-01 overlap difference RMS by observation period.

obs. 2 (3 h), obs. 3 (~4.5 h) and obs. 4 (~3 h). The resultant SLA-02 geolocation performance is worse than that obtained in support of SLA-01 due to much shorter arc lengths and tracking data distribution problems hampering POD, along with large amplitude, short duration attitude maneuvers during the observation periods. Residual and overlap RMS performance for all SLA-02 observation periods reprocessed are presented in Table 3. Due to the shorter arcs, a one revolution, 1.5-h, overlap duration was used. Again, solutions that simultaneously estimate orbit, pointing and range parameters from a combined reduction of navigation tracking data and laser altimeter surface range observations (solutions 2b and 3b) represent a significant improvement over the SLA-02 SDP (similar to solution 1b).

To understand the potential affects of range walk on our geolocation parameter solutions, the SLA-02 data were also reprocessed using waveform corrected ocean ranges in the solutions, and waveform corrected land observations for the final data geolocation. The ranges are corrected by analyzing the width of the received pulses taking into account the transmitted pulse width. For SLA, the transmitted pulse is not recorded and, therefore, an analysis was performed to estimate the pulse width. The pulse width from single peaked, high amplitude returns reflected from flat surfaces, were plotted as a function of amplitude and used to estimate the full pulse width at the threshold level above the background noise. Assuming a symmetric transmitted pulse, the half width has been estimated to be 7.5 m or 25 ns (http://denali.gsfc.nasa.gov:8001). Waveform corrected ranges were then reduced to the mean elevation recorded in the waveforms for ocean data, and to the lowest reached surface within the footprint for land data. The details of the SLA-02 waveform processing can be found in Carabajal et al. (1999). Results obtained from the processing of the waveform corrected ranges are shown in Table 3, solution 3b. Some improvement in orbit and geolocation height overlap comparisons is obtained while only minor degradations in direct altimeter range and horizontal geolocation precision performance are observed.

Fig. 6 summarizes the combined solution overlap performance for each of the observation periods studied. Observation period 1 performance is similar to that obtained in the SLA-01 analysis. This is the only SLA-02 observation period reprocessed in this study that had a good distribution of TDRSS tracking data and did not contain a significant attitude maneuver or loss of ocean surface returns. In contrast, observation period 2 had poor TDRSS tracking data distribution while period 4 contained a large amplitude, short duration, attitude maneuver which

Table 3

SLA-02 (data from observation periods 1, 2, 3 and 4) overlap and residual performance for various solution techniques

Solution		Data fit (RMS) Direct Alt. (m)	Orbit Overlap (RMS)		Geolocation Overlap (RMS)		
Solution number	Data		Radial (m)	Total (m)	Ht. ocean (m)	Ht. land + ocean (m)	Horiz. (m)
1b	a	3.86	5.60	14.35	3.18	3.84	409.28
2b	t + a	1.26	1.17	5.02	0.36	0.57	100.81
3b	t + a wvcor	1.28	1.01	4.75	0.33	0.46	104.75

Observation period dependent parameterization (see Table 1 for key). orb. is not estimated for "a" only run. Obs. 1, orb. + rbias + fullatt without the quadratic; Obs. 2, orb. + rbias + fullatt without the quadratic; Obs. 3, orb. + rbias + fullatt; Obs. 4, orb. + rbias + simpatt. wvcor, waveform corrected ranges.

degraded both orbit and geolocation overlap performance. The large amplitude and short duration attitude maneuver resulted in unmodeled residual attitude control system thrusting that degraded the POD performance and thereby affected the pointing parameter recovery. Observation period 3 contained some additional loss in ocean ranging data towards the end of the arc that affected the pointing parameter recovery. Nonetheless significant improvement in SLA-02 range residuals and orbit and geolocation precision have been obtained from the application of the combined solution technique.

3.2. The addition of dynamic crossovers in a combined solution with direct altimetry and spacecraft tracking data

In addition to the reduction of SLA-01 tracking and DA laser range data, SLA-01 ocean dynamic crossover (DXO) data were also analyzed. Tables 1 and 2 present the overlap and residual performance results obtained from a combined reduction of TDRSS tracking, DA and SLA-01-TOPEX/Poseidon (T/P) DXO data, where the crossovers are constructed from full-rate SLA-01 laser altimeter and T/P microwave altimeter surface return ranges (solution 5a). Again, the optimal data weighting and parameterization were determined using the overlap and residual performance metrics already discussed. A total of only 1097 SLA-01-T/P DXO observations were obtained over the 37 h of data reprocessed. While the inclusion of the few SLA-01-T/P DXOs only amounts to a very slight improvement in overlap performance, they do provide an excellent test of orbit and pointing performance and therefore resultant geolocation performance without the introduction of surface modeling errors. A frequency distribution of SLA-01-T/P DXO residuals is provided in Fig. 7. The DXO residuals show a significant improvement over the SLA-01 SDP (~solution 1a labeled *"a" best solution* in Fig. 7) has been obtained from the combined solution 4a (labeled *"t + a" best* in Fig. 7).
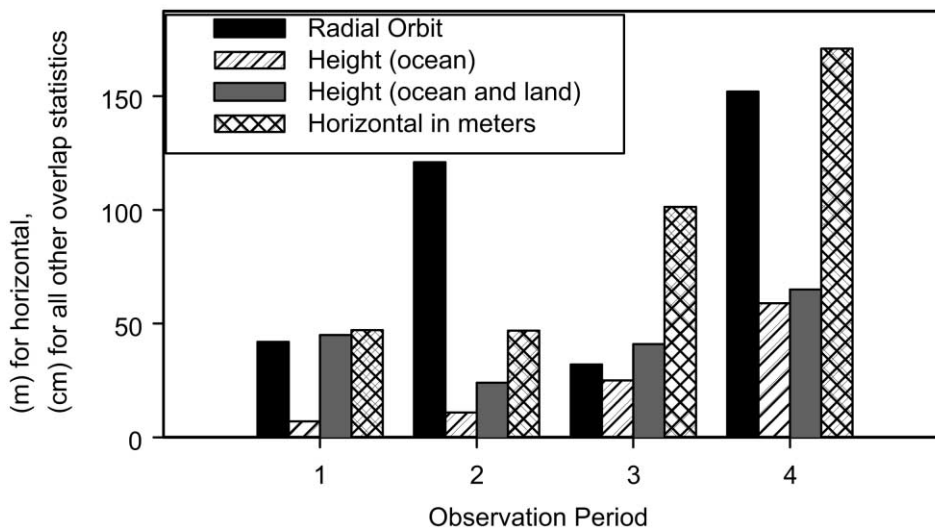

Fig. 6. SLA-02 overlap difference RMS by observation period (waveform corrected ranges).

The resultant DXO fits (Table 2 and Fig. 7) represent "somewhat" smoothed SLA range precision (T/P range precision < <SLA) without the effects of surface modeling errors. The SLA data has several periods were the data is not randomly distributed, but exhibits linear patterns or banding on the order of 1 second of data or less (Behn and Zuber, 2000). This hinders the DXO intrinsic smoothing from the polynomial fitting of the streams of altimeter range data. The recovery of timing biases, using the DXO data in a combination solution with tracking and DA data, was hampered by the SLA data characteristics. We were only able to resolve an observation timing bias to the 0.026 s (180 m horizontal) level using ocean DA and DXO data, and as discussed above, our observation timing bias is known to better than 0.010 s. In order to improve the results with the recovery of an observation timing bias, the timing bias resolution would need to be better than 0.005 s. In that case, ranging error signal less than 5 cm would need to be observed in the ocean data residuals. The 0.026 s timing bias resolution represents ranging error signal at the ~25–30 cm level which is the current level of systematic errors observed in the residuals after smoothing. Similarly, the recovery of an attitude timing bias did not improve the solution performance. Again this is due to the fact that the timing bias cannot be resolved to better than the current knowledge due to the limitation of the SLA ranging performance.

Even so, the DXO residuals indicate systematic pointing and orbit errors have been significantly reduced with the instrument ranging precision now dominating. Table 2 also presents SLA-01–SLA-01 DXO residual performance. Because there are so few SLA-01–SLA-01 DXO observations (140) available during this short mission, we have included these data from all observation periods studied and used them as a test of the solution 4a performance. These data fit
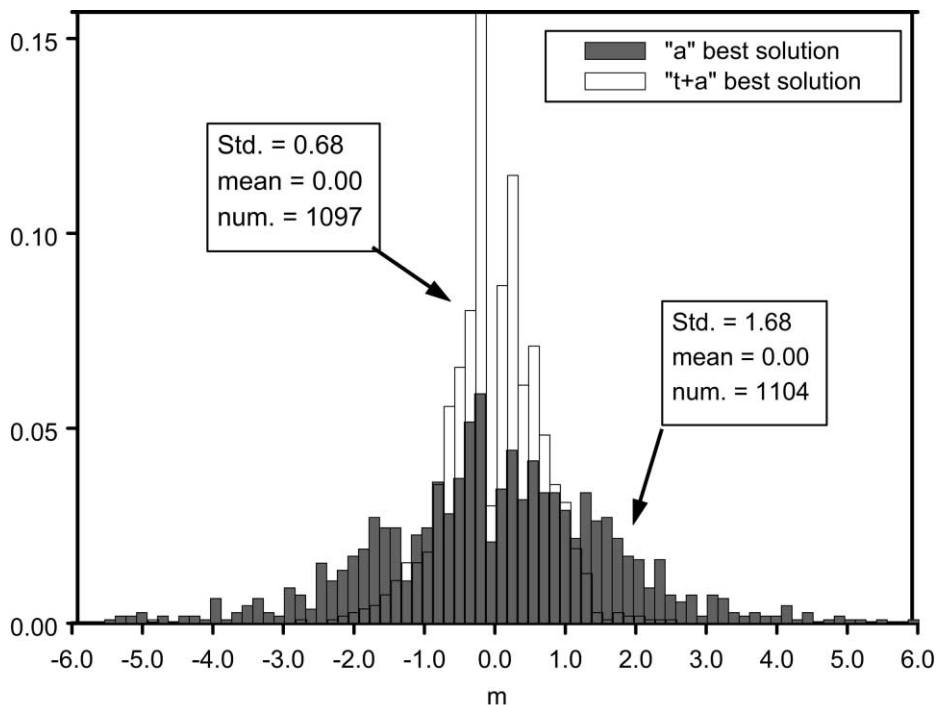

Fig. 7. SLA-01-T/P ocean crossover residual frequency (data from observation periods 1, 3s, 4 and 7).

to 99 cm RMS and again show the remaining residuals are dominated by instrument ranging precision because, in this SLA–SLA case, the ranging precision contribution to the residuals is multiplied by the square-root of two. For future missions, such as VCL and ICESat, the ranging performance will be on the level of 10 cm. With the improved system performance and a wealth of observations, it is expected that the DXO data will play an integral part in the recovery of geolocation parameters. This is especially true for VCL, where there are contiguous 25 m spots along-track so that there will always be a ''true'' crossover, and interpolation errors will be minimized, especially in rough, sloped and vegetated terrain. For ICESat's 172-m footprint spacing the crossovers will need to be interpolated leading to larger uncertainties for complex surfaces. VCL and ICESat inter-mission crossovers can be used to improve the performance of both missions, strengthen geolocation parameter solutions and to gauge the resultant geolocation accuracy. Additionally, accurate range data (DXO and DA) over undulating land topography will also strengthen the geolocation parameter solutions, especially timing biases. Both Neumann et al. (2001) and Rowlands et al. (1999) have performed detailed analyses that illustrate the power of using the crossover data to recover orbit, pointing, timing and ranging parameters in support of the Mars Orbiter Laser Altimeter data analysis. In this analysis, we have combined ''inter-'' and ''intra-mission'' DXO data with direct altimetry and spacecraft tracking. We have reduced the combination of these data and simultaneously recovered orbit, pointing, ranging and timing parameters to verify the algorithms and the combination solution methodology in preparation for the upcoming Earth observing laser altimeter missions VCL and ICESat.

3.3. SLA geolocation comparisons to DEMs

Although the GEODYN implementation of the DA measurement model allows us to compute and reduce range residuals to a gridded Digital Elevation Model (DEM) in a combined solution, we have chosen to apply these DEM comparisons as an independent gauge of geolocation accuracy. To assess the horizontal accuracy of the various geolocation solutions, individual laser altimeter surface profiles are matched to available raster DEM derived topographic profiles, and estimates of the track horizontal offsets that minimize the height differences are computed. This approach, applying shifts in the horizontal X and Y directions, has been used to evaluate the SLA-01 and SLA-02 geolocation Enhanced Data Product (EDP) solutions 4a, 2b and 3b, obtained from the above analysis. Sub-orbital track segments representing orthometric elevations for the footprint locations are differenced with the corresponding DEM. The position of the profile is systematically shifted with respect to the DEM in the North-South and East-West directions. The optimal shift necessary to minimize the elevation differences indicates the most suitable location for the profile on the surface of the Earth. The DEM needs to be extensive enough to include a sufficient number of footprint elevations, possess sufficient accuracy, and have enough resolution to enable meaningful interpretation of the results. The topographic profiles needed to include a certain degree of complexity for the comparisons to give rise to a well-constrained minimum in the residual space. The most important factors that influence the statistical power of the technique are the number of points included in the profile considered, and its ability to represent a diverse type of terrain. Trade-offs between the characteristics of the DEM and the profile's characteristics that influence these comparisons and their ability to resolve regional geolocation ambiguities for a profile segment exist.

Two raster DEM data sources were used: the Digital Terrain Elevation Data Level 1 (DTED1) gridded at 3 arc-s (approximately 90 m) produced by the U.S. National Imaging and Mapping Agency (NIMA), and the seamless National Elevation Dataset (NED), assembled by the U.S. Geological Survey with a 1 arc-s (approximately 30 m) resolution that has recently become available (http://gisdata.usgs.gov/ned). The DTED1 accuracy is known to vary geographically and with method of production; the specified absolute vertical accuracy (90% linear error) is 30 m (18 m RMSE) (Harding et al., 1999). It was gridded using the World Geodetic System 1984 (WGS-84). The NED data set's vertical accuracy was initially assessed at $\sim$3.74 m RMSE based on 5811 National Geodetic Survey (NGS) control points (Gesch, pers. comm.). For the solutions corresponding to SLA-01 arcs, only first return profiles (ranging to the highest surface within the footprint) were compared. Since the SLA-02 range data corrected for waveform information were also processed in this analysis, comparisons were also performed with these data representing geolocation of the lowest surface intercepted within the footprint. In these cases, data were limited to where waveform data were successfully processed and no significant waveform jitter was present. SLA orthometric heights were computed by subtracting the geoid values at the footprint locations using Earth Geoid Model-96 (EGM-96) (Lemoine et al., 1998). Only data that represented valid altimetric observations were included in these comparisons, constraining the available data to elevations that were within 100 m of the interpolated DEM value. This way, a significant number of laser returns that were intercepted by clouds were eliminated, although in some cases the profiles reflected the presence of orographic clouds near mountain fronts that had remained (not been edited), adversely influencing the comparison.

For most comparisons, shifting of the altimetric profile was done in increments equal to the grid resolution. Shifting at sub-grid increments was also done to test the resulting improvement in the solution resolution. Elevation residual RMS contours are used to illustrate the convergence of the solution to an optimal minimum for every case. Mean and standard deviation of the elevation differences were also computed. The potential and effectiveness of this technique is illustrated in Fig. 8. Solutions 1a and 4a for SLA-01 first return data have been tested for their accuracy against DTED1 at 3 and 1 arc-s increments. The residual RMS contour plots reveal the progressive improvement (from solution 1a to 4a) in the match between the geolocation of the laser profile and the corresponding DTED1 profile. Sub-sampling of the DEM at 1 arc-s increments increases the strength of this technique in discriminating between solutions while giving a more precise estimate of the optimal horizontal shift. Therefore, a more accurate estimate of the horizontal errors is obtained when 1 arc-s increments are used. Table 4 shows these results for SLA-01 data vs. DTED1 for various regions. Profiles contained between 300 and 1300 footprint elevations.

For the "clean" SLA-01 observation periods (1, 3s, 4), Table 4 shows the improvement in horizontal accuracy of 93.77 m for solution 1a, to 60.88 m for solution 4a. These results agree nicely with the improvements observed in overlap and residual RMS performance as presented above (Tables 1 and 2 and Figs. 2, 4, 5 and 7) and summarized here: 93.24 m RMS horizontal precision for solution 1a and 39.54 m RMS horizontal precision for solution 4a from geolocation overlap analysis. The small discrepancies between the DEM profile comparisons and the overlap analysis results are due to several factors including: (1) the profile comparisons only test a very small, limited amount of the solution's data and do not represent a good sampling of the arc, (2) systematic errors still exist (e.g., timing biases) that are not observed in the precision estimates.

However, these results show that the combined solution 4a not only represents significant improvement in geolocation precision and residual performance, but also represents significant improvement in these accuracy tests. From the analysis conducted and the stated vertical accuracies of the DEMs, the large elevation differences are dominated by the accuracy characteristics of the particular DEMs compared. Not accounting for the vertical biases in the comparisons may cause them to bleed into errors in the horizontal positioning, and can be reflected in the estimated optimal shifts calculated for the present comparisons. This stresses the need to solve for vertical biases as well. Implementation of shifting in the vertical direction in conjunction with the horizontal shifting is being developed at present, and will be tested with these and other applicable data sets in the future. Still, these comparisons provide a good assessment of the horizontal geolocation accuracy. The observation period 7 profile comparisons presented in Table 4 also show the degradation in horizontal geolocation performance observed
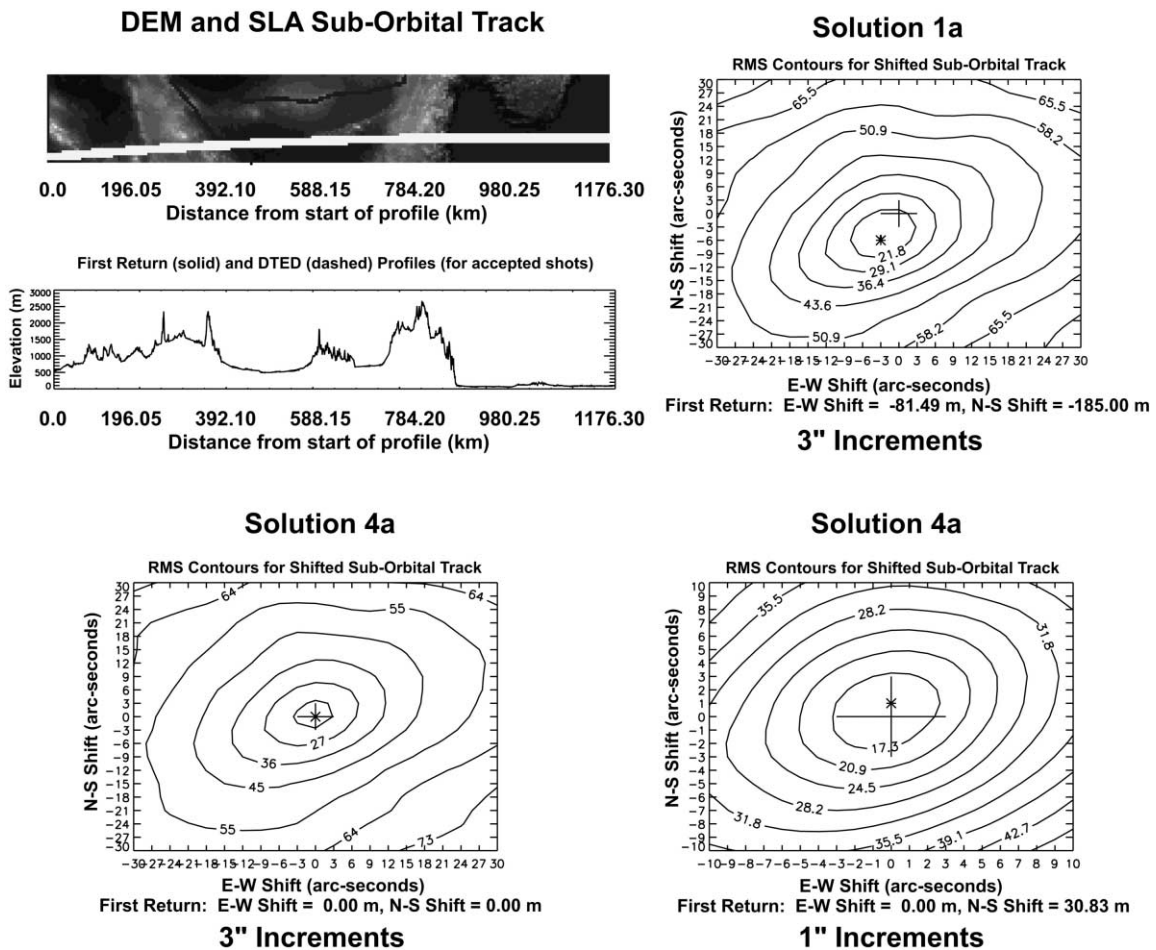

Fig. 8. SLA-01 observation period 4 suborbital track segment compared to 90m Asia DTED for different solution types and shifting increments.

in the residual and overlap comparisons for this observation period. As mentioned in the above analysis, this observation period suffered from poor TDRSS tracking data distribution, which affected POD and pointing correction recovery. However, even for this anomalous arc, significant improvements are observed in accuracy from the combined solution 4a. The lower horizontal shift average value (Table 4), for the 3 arc-s increments, results from the inability to resolve accuracy below the grid cell level, showing that no shift or smaller shifts were necessary for more of the comparisons than when 1 arc-s increments were used and a more accurate result can be obtained.

Two Maryland, US areas (labeled A and B in Table 5) were used in DEM comparisons of SLA-02 observation period 2 profiles. First and last return profiles for the previously distributed SLA-02 SDP-V2 (Standard Data Product Version 2) data sets were compared to DTED1 in area A. Horizontal shift estimates were found to be 185 m for the SDP-V2 in Maryland for observation period 2 (comparison #1, Table 5). Table 5 also shows the results of the comparisons between observation 2 EDP (solutions 2b and 3b) tracks against area A (#2 and #3) where the horizontal shift estimates have been improved to 71 m. These results indicate significant improvement in horizontal geolocation accuracy has been achieved using the combination EDP solutions (2b and 3b). Additionally, Table 5 presents Maryland Area B (#4–9) DEM comparisons of the preferred EDP geolocation solutions with and without applying waveform corrections (solutions 2b and

Table 4
Selected SLA-01 sub-orbital track segments compared to DTED1 using 3 or 1 arc-s shifting increments for various geographic regions

Observation period	Area	Elevation Differences by Solution Type, Mean±STD (m)			Horizontal Shift by Solution Type, RSS (m)		
		1a (3″)	4a (3″)	4a (1″)	1a (3″)	4a (3″)	4a (1″)
Obs. 1	C.Africa	11.71±11.80	9.56±12.43	10.00±12.10	0.00	0.00	43.56
Obs. 1	India1	0.50±15.85	2.85±15.73	2.85±15.71	92.5	0.00	30.83
Obs. 1	India4	3.77±11.73	5.21±11.76	5.23±11.55	125.87	0.00	64.72
Obs. 1	S.America1	11.56±18.48	11.03±19.93	10.90±18.96	81.42	0.00	41.07
Obs. 3s	S.Arabia7	13.37±14.10	13.65±14.37	13.45±12.39	92.5	92.50	67.35
Obs. 3s	N.E.Africa6	15.30±13.28	14.34±13.54	14.30±13.14	124.22	0.00	30.83
Obs. 3s	N.E.Africa7	12.37±12.90	11.49±12.59	11.46±12.27	92.5	92.50	67.47
Obs. 4	M.E.2	11.33±15.91	14.54±15.59	14.74±14.74	82.21	92.50	96.47
Obs. 4	S.America1	15.61±19.73	15.61±19.02	14.94±18.26	92.5	123.22	82.15
Obs. 4	S.America2	16.85±19.53	14.39±20.87	15.02±19.32	123.56	123.56	82.37
Obs. 4	Africa12	−2.22±7.44	−0.09±7.49	−0.07±7.42	124.22	82.16	62.85
Average (m)		**10.01**	**10.23**	**10.26**	**93.77**	**55.13**	**60.88**
Obs. 7	M.E.3	9.96±16.34	10.08±16.32	10.13±15.93	202.45	185.00	154.17
Obs. 7	India1	6.0±9.22	6.10±9.22	6.16±9.19	185.00	92.50	97.07
Obs. 7	India6	4.60±11.08	5.89±10.88	5.68±10.22	185.00	92.50	156.69
Obs. 7	Africa18	9.33±19.63	9.35±20.00	9.33±19.87	204.05	92.50	126.62
Obs. 7	S.America3	20.64±18.40	19.88±17.71	19.88±17.71	83.66	83.66	83.66
Average (m)		**10.11**	**10.26**	**10.24**	**172.03**	**109.23**	**123.64**

Table 5
Comparisons of SLA-02 observation period 2 sub-orbital track segments for two regions in Maryland, US

SLA02 Observation 2 (Geolocation Solution)		DEM and Shifting Interval (arc-s)	Number of Points	Elevation Difference Mean±STD	Horizontal Shift RSS (m)
Area A					
#1	First Return (SDP-V2, ~1b)	DTED1 (3)	344	9.59 ±9.59	185.0
#2	First Return (2b)	DTED1 (3)	338	8.22 ±9.84	71.38
#3	Last Return (3b)	DTED1 (3)	193	−6.20 ±6.02	71.38
Area B					
#4	First Return (2b)	DTED1 (3)	304	10.51 ±10.07	72.13
#5	First Return (2b)	DTED1 (1)	304	10.51 ±10.07	72.13
#6	First Return (2b)	NED (1)	304	12.67 ±11.57	57.12
#7	Last Return (3b)	DTED1 (3)	148	−6.56 ±5.55	72.14
#8	Last Return (3b)	DTED1 (1)	148	−6.47 ±5.46	78.45
#9	Last Return (3b)	NED (1)	148	−4.59 ±6.49	72.14
Average values (m)				2.26	70.86

3b). Area B corresponds to a region where equivalent NED cells were available from our initial data request. Waveform processing constraints have reduced the number of points included in the waveform-corrected profiles. Shifts in the horizontal direction were performed at 3 and 1 arc-s resolution. Results of comparisons against NED are shown in Table 5, and illustrated in Fig. 9 (results of comparison #6). This profile matching analysis is not always able to discern whether first or last return solutions were better based on the estimated necessary horizontal shift. However, improvement in the solutions can be seen in the elevation differences mean and standard deviation improvement. Comparisons against the waveform-corrected data show the influence that a reduced sampling of footprint elevations has in resolving the optimal shift along a profile segment. Nevertheless, the profile matching analysis clearly shows a significant improvement in geolocation accuracy has been obtained from the combined solution 2b or 3b, as has been shown with overlap and residual performance tests previously discussed. Again, it should be noted that the profile matching only compares a very small sample of the entire geolocated data and can not be used as an overall accuracy assessment, but should be used in conjunction with overlap and residual (DA and DXO) performance to give an indication of the final geolocation accuracy.

While the DEM profile comparisons, overlap and residual analyses will provide a means to assess the intermediate and long wavelength geolocation errors, a waveform matching technique will be used to assess the shot-to-shot geolocation errors due to effects such as laser pointing knowledge jitter (Blair and Hofton, 1999). Synthesized waveforms constructed from very high resolution DEMs are compared to the observed waveforms where the correlation is optimized by estimating horizontal and geolocation offsets on a shot-by-shot basis. This technique can also be used to validate observed surface characteristics (i.e., slope and surface roughness) and fundamental laser characteristics such as footprint diameter, circularity and pulse width (Blair and Hofton, 1999).
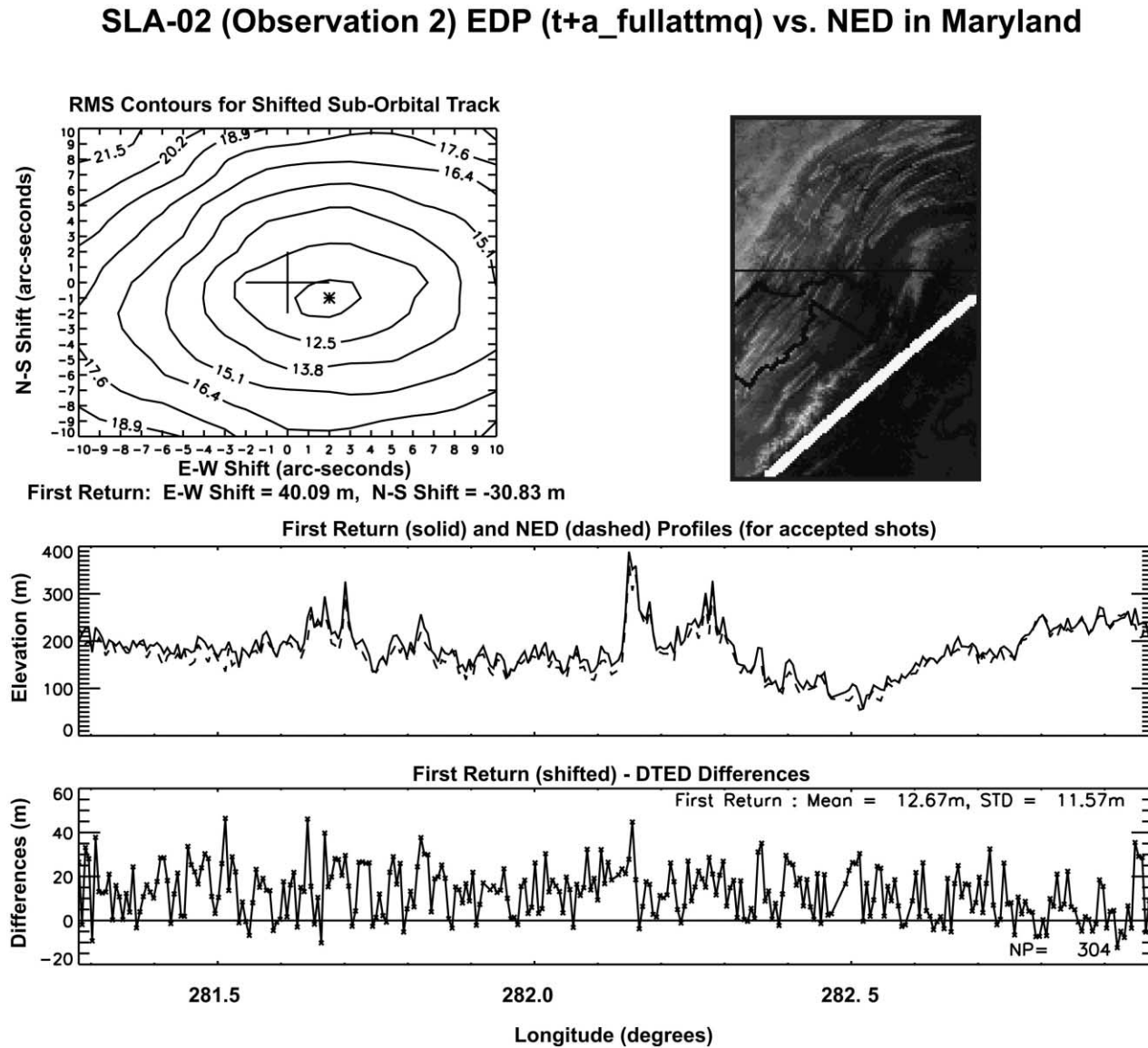
SLA-02 (Observation 2) EDP (t+a_fullattmq) vs. NED in Maryland

Fig. 9. SLA-02 EDP for observation 2 without waveform correction compared to National Elevation Data (NED) derived elevations.

4. Concluding remarks

In preparation for NASA's dedicated spaceborne laser altimeter missions, VCL and ICESat, detailed algorithms and methodologies have been developed and tested to precisely geolocate the surface return of the reflected laser energy. To properly geolocate these surface bounce points, it is necessary to compensate for pointing, ranging, timing and orbit errors. These geolocation parameters will have to be estimated and validated once on orbit. Towards this end, rigorous laser direct altimetry, dynamic crossover and geolocation measurement models have been implemented within NASA's state of the art precision orbit determination and geodetic parameter estimation software, GEODYN. These algorithms provide an integrated range residual analysis capability to simultaneously estimate orbit, pointing, ranging and timing geolocation parameters from a combined reduction of direct altimetry, dynamic crossover and spacecraft tracking data resulting in an enhanced geolocation product.

Several pre-launch error analyses have been performed that show the power of the integrated range residual analysis technique in producing an enhanced geolocation product. However, it is also important to rigorously test these algorithms and to develop an analysis methodology using real Earth observing spaceborne laser altimeter data. The data from the SLA missions provided an excellent pathfinder data set to test our algorithms and processes and to develop our geolocation analysis methodology. Data from several SLA-01 and SLA-02 observation periods, representing a good sampling of the mission data, have been reprocessed using our algorithms, software and analysis methodologies. Residual and overlap performance have been used as metrics to determine the optimal data weighting (tracking and altimetry) and orbit, pointing, ranging and timing parameterization. Significant improvements in geolocation have been achieved from a combined reduction of laser altimeter range observations and spacecraft tracking data simultaneously estimating pointing, ranging and orbit parameters. Inter-mission dynamic crossovers with T/P have been used to contribute to the orbit and geolocation parameter recovery, and both inter- and intra-mission crossovers have been used to assess the solution performance. Resultant SLA-01 enhanced geolocation precision is on the order of 40 m RMS horizontal and 26 cm RMS in elevation. DEM profile accuracy assessments show similar performance at 60-m horizontal positioning. Ocean range residuals show the SLA ranging performance is now at the 1-m level. Overall improvement over the SLA-01 SDP geolocation is nearly a factor of two. Orbit precision and accuracy have also been improved by more than a factor of 2 over the SDP orbits and are at the 30-cm radial RMS level. Detailed analysis of SLA-02 enhanced data geolocation, also obtained from a combined solution, show significant improvement in resultant overlap, residual and DEM profile comparison performance. Finally, the analysis presented in this paper shows that complex temporal variations in pointing, and not just simple biases, can be precisely recovered.

While the shuttle is not a geodetic satellite and the SLA does not possess the ranging performance that both VCL and ICESat will achieve, the data have been invaluable in developing, validating and assessing our processing algorithms, software and methodologies. Furthermore, when taking into account the SLA data limitations, the results achieved in this analysis show that the techniques applied here can meet VCL and ICESat required geolocation performance. A truly combined calibration solution for VCL and ICESat geolocation parameters can be made processing direct altimetry from "ocean sweeps" and detailed land calibration sites along with land

and ocean dynamic crossover and spacecraft tracking data. Furthermore, inter-mission VCL and ICESat DXO data will be applied to strengthen geolocation parameter solutions and to improve the geolocation performance. The VCL contiguous along-track footprints will result in improved DXO performance and may be used to improve ICESat geolocation performance and validation. The data over the course of the entire mission can be used to recover long term variations in pointing and ranging parameters due to aging of systems and long period environmental influences. The orbits for both VCL and ICESat will be precisely determined from dual frequency GPS data and will likely not benefit from the addition of laser altimeter data to the POD. However, in the event of a GPS receiver failure, or periods of data loss, it will be important to have the capability to combine the altimeter range data with satellite laser ranging (SLR) for the POD. Unlike ICESat, VCL also has the capability of acquiring TDRSS tracking. Pre-launch error analyses show that in the event of a GPS failure we can begin to approach VCL minimum science mission geolocation requirements if we perform a combined reduction of TDRSS, SLR and the laser altimeter range data. The optimal altimeter and tracking data weighting and orbit and geolocation parameterization will be found using the same metrics and methodologies developed here for the SLA analysis. The resultant geolocation will be validated using DEM profile comparisons to assess long wavelength errors, and the Blair and Hofton (1999) waveform matching technique to assess shot-to-shot geolocation errors. The wealth of data collected from VCL's airborne simulator instrument, the Laser Vegetation Imaging Sensor (LVIS), will be used in these geolocation calibration and validation analyses (Blair et al., 1999).

References

Behn, M.D., Zuber, M.T., 2000. A comparison of ocean topography derived from the shuttle laser altimeter-01 and TOPEX/POSEIDON. IEEE Transactions on Geoscience and Remote Sensing 38 (3), 1425–1457.

Bertiger, W., Bar-Sever, Y., Desai, S., Duncan, C., Haines, B., Kuang, D., Lough, M., Reichert, A., Romans, L., Srinivasan, J., Webb, F., Young, L., Zumberge, J., 2000. Precise orbit determination for the shuttle radar topography mission using a new generation of GPS receiver. In: Proceedings of ION GPS, Salt Lake City, UT.

Blair, J., 1999. B, Hofton, M. A., Modeling laser altimeter return waveforms over complex vegetation using high-resolution elevation data. Geophysical Research Letters 26, 2509–2512.

Blair, J.B., Rabine, D.L., Hofton, M.A., 1999. The laser vegetation imaging sensor: a medium-altitude, digitization-only, airborne laser altimeter for mapping vegetation and topography. ISPRS Journal of Photogrammetry & Remote Sensing 54, 115–122.

Bufton, J.L., 1989. Laser altimetry measurements from aircraft and spacecraft. Proceedings of the IEEE 77 (3), 463–477.

Carabajal, C.C., Harding, D.J., Luthcke, S.B., Fong, W., Rowton, S.C., Frawley, J.J., 1999. Processing of Shuttle Laser Altimeter Range and Return Pulse Data in Support of SLA-02. International Archives of Photogrammetry and Remote Sensing 32 (3214), 65–72.

Dubayah, R., Blair, J.B., Bufton, J.L., Clark, D.B., JaJa, J., Knox, R., Luthcke, S.B., Prince, S., Weishampel, J., 1997. The Vegetation Canopy Lidar Mission. Land Satellite Information in the Next Decade II: Sources and Applications. American Society for Photogrammetry and Remote Sensing, Bethesda, MD.

Fu, L.L., Pihos, G., 1994. Determining the response of the sea level to atmospheric pressure forcing using TOPEX/POSEIDON data. Journal of Geophysical Research 99 (C12), 24,633–24,642.

Gardner, C.S., 1992. Ranging performance of satellite laser altimeters. IEEE Transactions on Geoscience and Remote Sensing 30 (5), 1061–1072.

Garvin, J.B., Bufton, J.L., Blair, J.B., Harding, D.J., Luthcke, S.B., Frawley, J.J., Rowlands, D.D., 1998. Observations of the Earth's topography from the shuttle laser altimeter (SLA): laser pulse echo-recovery measurements of terrestrial surfaces. Physics and Chemistry of the Earth 23 (9–10), 1053–1068.

Harding, D.J., Gesch, D.B., Carabajal, C.C., Luthcke, S.B., 1999. Application of the shuttle laser altimeter in an accuracy assessment of GTOPO-30, a global 1-kilometer digital elevation model. International Archives of Photogrammetry and Remote Sensing 32 (3W14), 81–85.

Hitchhiker CARS (Customer Accommodations and Requirements Specifications), 1994. HHG-730-1503-07. Goddard Space Flight Center, Greenbelt, Maryland.

Lemoine, F.G., Kenyon, S.C., Factor, J.K., Trimmer, R.G., Pavlis, N.K., Chinn, D.S., Cox, C.M., Klosko, S.M., Luthcke, S.B., Torrence, M.H., Wang, Y.M., Williamson, R.G., Pavlis, E.C., Rapp, R.H., Olson, R.H., 1998. The Development of the Joint NASA GSFC and the National Imagery and Mapping Agency (NIMA) Geopotential Model EGM96. NASA Technical Memorandum, NASA/TP-1998-206861, Goddard Space Flight Center, Greenbelt, MD.

Luthcke, S.B., Carabajal, C.C., Rowlands, D.D., Pavlis, D.E., 2002. Improvements in spaceborne laser altimeter data geolocation. Surveys in Geophysics, 22 (5–6).

Luthcke, S.B., Rowlands, D.D., McCarthy, J.J., Pavlis, D.E., Stoneking, E., 2000. Spaceborne laser-altimeter-pointing bias calibration from range residual analysis. Journal of Spacecraft and Rockets 37 (3), 374–384.

Luthcke, S.B., Marshall, J.A., Rowton, S.C., Rachlin, K.E., Cox, C.M., Williamson, R.G., 1997. Enhanced radiative force modeling of the tracking and data relay satellites. The Journal of the Astronautical Sciences 45 (3), 349–370.

Neumann, G.A., Rowlands, D.D., Lemoine, F.G., Smith, D.E., Zuber, M.T., 2001. Crossover analysis of Mars Orbiter laser altimeter data. Journal of Geophysical Research 106 (E10), 23753–23768.

Pavlis, D.E., Moore, D., Luo, S., McCarthy, J.J., Luthcke, S.B., 1999. GEODYN Operations Manual: 5 volumes. Raytheon ITSS, Greenbelt, MD.

Ray, R.D., 1999. A Global Ocean Tide Model from TOPEX/Poseidon altimetry:GOT99.2. NASA Technical Memorandum, 209478. Goddard Space Flight Center, Greenbelt, MD.

Rowlands, D.D., Carabajal, C.C., Luthcke, S.B., Harding, D.J., Sauber, J.M., Bufton, J.L., 2000. Satellite laser altimetry: on-orbit calibration techniques for precise geolocation. The Review of Laser Engineering 28 (12), 796–803.

Rowlands, D.D., Pavlis, D.E., Lemoine, F.G., Neumann, G.A., Luthcke, S.B., 1999. The use of laser altimetry in the orbit and attitude determination of Mars Global Surveyor. Geophysical Research Letters 26 (9), 1191–1194.

Rowlands, D.D., Luthcke, S.B., Marshall, J.A., Cox, C.M., Williamson, R.G., Rowton, S.C., 1997. Space Shuttle precision orbit determination in support of SLA-1 using TDRSS and GPS tracking data. The Journal of the Astronautical Sciences 45 (1), 113–129.

Wunsch, C., Stammer, D., 1995. The global frequency-wavenumber spectrum of oceanic variability estimated from TOPEX/POSEIDON altimetric measurements. Journal of Geophysical Research 100 (C12), 24,895–24,910.

Yi, Y., 1995. Determination of Gridded Mean Sea Surface from TOPEX, ERS-1 and GEOSAT Altimeter Data. Report No. 434. The Ohio State University, Columbus, OH.

Zwally, H.J., Schutz, B., Abdalati, W., Abshire, J., Bentley, C., Brenner, A., Bufton, J., Dezio, J., Hancock, D., Harding, D., Herring, T., Minster, B., Quinn, K., Palm, S., Spinhirne, J., Thomas, R., 2002. ICESats Laser measurements of polar ice, atmosphere, ocean. Journal of Geodynamics 34, 405–445